DIAGNOSIS OF INTER-TURN SHORT CIRCUIT FAULT IN INDUCTION MACHINE

Andrian CEBAN [1,2], Remus PUSCA [1,2], Raphael ROMARY [1,2] and Jean-Philippe LECOINTE [1,2]

[1] Univ Lille Nord de France, F-59000 Lille, France
[2] UArtois, LSEE, F-62400 Béthune, France
E-Mails: apceban@gmail.com; puscaremus@hotmail.com;
raphael.romary@univ-artois.fr; jphilippe.lecointe@univ-artois.fr

***Abstract* – This paper describes a new non-invasive method for the fault diagnosis of inter-turn short circuit in induction machine. The proposed diagnosis procedure is based on the analysis of the external magnetic field in the machine's vicinity and more particularly its space variations measured by two coil sensors. The principle consists in the comparison of the specific harmonic magnitude whether the machine runs under no-load or load conditions. Its main interest consists in the fact that the load operation does not constitute any more a perturbing factor but rather it corresponds to an essential state allowing failure discrimination.**

In this context, an analytical modeling which describes an elementary damaged coil of a four pole induction machine is presented. It is shown how this fault can be effectively diagnosed by the use of the non-invasive approach. Then, the 2D finite element analysis is performed for studying the influence of stator turn fault on the machine. This analysis is focused especially on the specific frequency component of the magnetic field.

In order to validate the proposed method, a special three-phase induction machine has been designed and constructed to simulate the incipient stator winding faults. The obtained experimental results clearly validate the analytical and simulation results.

***Keywords*:** *induction machine, inter-turn short circuit, fault diagnosis, finite element analysis, magnetic flux density, spectral analysis.*

1. INTRODUCTION

Many works existing in literature have shown that a large percentage of failures in an induction machine result from a fault related to the stator winding and core. For example, the inter-turn short circuit in stator windings represent 30%–40% of the existing faults in induction machines [1, 2]. In the most cases the inter-turn fault is caused by thermal, thermo-mechanical, vibrational and environmental stresses during operation, and also by partial discharge, presented in electrical machines supplied by inverters [2-4].

During the past two decades, there has been a substantial amount of research into the creation and developing of new condition monitoring techniques for electrical machine drives [1, 5]. The research and development of newer and alternative diagnostic techniques are continuous [6, 7]. They have moved from traditional techniques to artificial intelligence techniques [8]. An ideal diagnostic procedure should take the minimum measurements in order to give a clear indication of incipient failure modes in a minimum time. In most part, the non-invasive methods by relying on easily measured electrical quantities like current [9-11], voltage and flux [12-15] can assure that. Methods based on the external magnetic field analysis have been developed in the past few years; their advantage lays in the simplicity of implementation. Generally, these methods are based on the comparison between a reference spectrum corresponding to a healthy state and a given one measured during the machine operating.

The study presented in this paper shows a new signature for inter-turn fault diagnosis in the frequency spectrum of the external magnetic field. Contrary to classical methods, the presented method does not require any knowledge of a presumed machine's healthy former state and the load is not a disturbing factor but it is used as the fault discrimination. The originality consists in the comparison of the delivered sensor signals according whether the machine runs under no-load and load conditions.

Initially, an analytical study to describe elementary damaged coil model is presented. Then the 2D finite element model of the induction machine is used to compute the harmonics of the external magnetic field.

Finally, a modified induction machine is used to make the tests in order to validate the proposed method.

2. MODELING OF INTER-TURN SHORT CIRCUIT

For this study, it is used a four pole induction machine ($p = 2$). Based on the analytical model described in [13], one suppose that y turns among n^s / m^s of an elementary coil of the phase q are short-circuited (where m^s – number of elementary coils and

n^s – the machine per phase, per pole pair turn number). If y is small compared to pn^s it is possible to consider that the i_q^s currents are unchanged (see Figure 1). This assumption makes it possible to characterize short-circuit fault by implementing a model which preserves the initial structure of the machine. This model considers that the faulty stator winding is equivalent to the healthy winding, plus y short-circuited turn coil which is denoted "additional coil". In this coil circulates a i_{qf}^s fictitious current composed of short-circuit induced current i_{sc}^s and the i_q^s current in opposite direction:

$$i_{qf}^s = i_{sc}^s - i_q^s \tag{1}$$

2.1. Elementary damaged coil model

An elementary damaged coil is given in Figure 1. This approach makes it possible to separate the effects of the fault while preserving the initial structure, what simplifies the fault analysis.

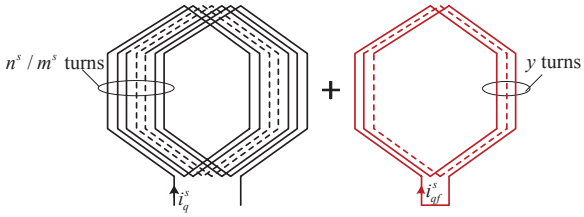

Figure 1: Elementary coil with y short-circuited turns.

The resulting air-gap flux density b^* can be expressed as:

$$b^* = b + b_{qsc}^s \tag{2}$$

with:

$$b = \sum_{K,H} b_{K,H} = \sum_{K,H} \hat{b}_{K,H} \cos\left(K\omega t - H\alpha^s - \varphi_{K,H}\right) \tag{3}$$

where K is the frequency rank and H – pole pair number of $b_{K,H}$ and b_{qsc}^s is the flux density generated by the damaged coil, ω is the angular frequency, α^s angular gap between the stator reference and a point located in the air-gap. $\varphi_{K,H}$ is the phase which depends on the position of the elementary coil concerned by the short-circuit but also of the phase where the short-circuit occurs.
Under healthy conditions the quantities K and H in the case of induction machine can be expressed by:

$$\left.\begin{aligned} K &= 1 + k^r N^r (1-s) \\ H &= p\left(h^s + k^s N^s + k^r N^r\right) \end{aligned}\right\} \tag{4}$$

where s is the slip, h^s is a not null relative integer, which takes among others, all the values of h^s which is defined by: $h^s = 6k+1$, where k is an integer number which varies between $-\infty$ to $+\infty$, k^s is a coefficient corresponding to stator and k^r is a coefficient corresponding to rotor; N^s is the stator per pole pair tooth numbers and N^r is the rotor per pole pair tooth numbers.
The flux density b_{qsc}^s generated by the fault is obtained by multiplying the magneto motive force (MMF) generated by the additional coil (it is a unidirectional wave) with air-gap permeance:

$$b_{qsc}^s = \sum_{K_{sc},H_{sc}} \hat{b}_{sc_{K_{sc},H_{sc}}} \cos\left(K_{sc}\omega t - H_{sc}\alpha^s - \varphi_{sc_{K_{sc},H_{sc}}}\right) \tag{5}$$

with the sensitive lines to the fault are characterized by the quantities K_{sc} and H_{sc} defined as follows:

$$\left.\begin{aligned} K_{sc} &= 1 + k'^r N^r (1-s) \\ H_{sc} &= h + p\left(k'^s N^s + k'^r N^r\right) \end{aligned}\right\} \tag{6}$$

k'^s and k'^r corresponding to the fault case, are equivalent to k^s and k^r. Consequently they vary from $-\infty$ to $+\infty$.
The resulting flux density appears, after attenuation, at the level of the external transverse field. That results in the presence of harmonics at $K\omega$ and $K_{sc}\omega$ angular frequencies in the signal delivered by the flux sensor. Considering K and K_{sc} the values calculated by (4) and (6), it is possible to make the following remark: K_{sc} does not bring new frequencies and the failure presence will be appreciated through the variation of the amplitudes of existing lines in the healthy machine spectrum.
These properties make difficult the diagnosis by analysis of the changes in the amplitudes of the measured components. In the following the properties relating to the dissymmetry generated by the fault will be exploited.

2.2. Presentation of the Proposed Method

The measurements are carried out in two diametrically opposed positions (see Figure 2): $\alpha^s = \beta_0$ (Position 1) and $\alpha^s = \beta_0 + \pi$ (Position 2).
The principle of the method consists in the analysis of the variations induced by the fault at the level of particular harmonic components measured in the both positions. The corresponding flux density components must have significant amplitude in the external magnetic field.

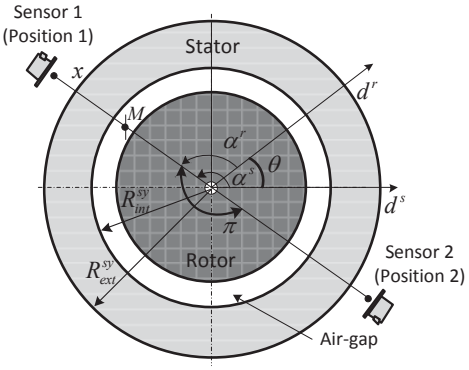

Figure 2: Simplified section of a machine

The $K\omega$ component of the flux linked by the coil sensor results from:

$$\Psi_K^x = \int_S b_K^x dS \tag{7}$$

with: $\hat{b}_{K,H}^x = \kappa_H^{sy} \hat{b}_{K,H}$.

The transverse external flux density is deduced from b in (3), through an attenuation coefficient κ_H^{sy} tied to the stator yoke only [16]. This coefficient can be written as following:

$$\kappa_H^{sy} = \frac{2}{\left(\mu_r^{sy}+1\right)\left(R_{int}^{sy}/R_{ext}^{sy}\right)^{-H-1} - \left(\mu_r^{sy}-1\right)\left(R_{int}^{sy}/R_{ext}^{sy}\right)^{H-1}} \tag{8}$$

where μ_r^{sy} is the relative magnetic permeability of the stator yoke material, R_{int}^{sy} and R_{ext}^{sy} are the internal, respectively external radius of stator yoke (laminations).

Figure 3 gives in log scale the variation of κ_H^{sy} for $\mu_r^{sy} = 1000$, $R_{int}^{sy} = 0.0825\,\text{m}$ and $R_{ext}^{sy} = 0.121\,\text{m}$.

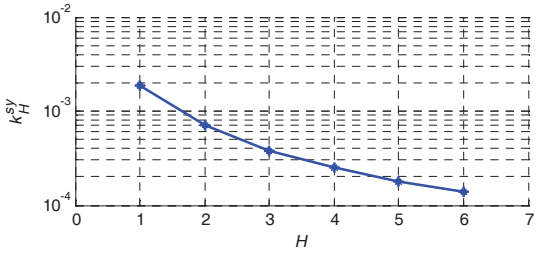

Figure 3: Variation κ_H^{sy} versus H

The attenuation coefficient depend only H , the pole pair number of the considered flux density component. One can observe that it decreases when H increases.

The result of integration (7) depends of the sensor parameters (turns number n^c and sensor area S), but also of H and x . Introducing these parameters in the coefficient K_H^x , Ψ_K^x is expressed by:

$$\Psi_K^x = \sum_H \kappa_H^{sy} K_H^x \hat{b}_{K,H} \cos\left(K\omega t - H\beta_0 - \varphi_{K,H}^x\right) \tag{9}$$

$\varphi_{K,H}^x$ results from $\varphi_{K,H}$ by taking into account the phase change possibly introduced by the eddy currents.

Among the components which constitute Ψ_K^x only few of them, relative to low pole number (low H), have a significant contribution. The other components will be absorbed by the ferromagnetic parts of the machine. The EMF e^x delivered by the sensor is given by:

$$e^x = \sum_K \hat{e}_K^x \sin\left(K\omega t - \varphi_{K,H}^x\right) \tag{10}$$

with:

$$\begin{aligned} \hat{e}_K^x &= -K\omega \left| \sum_H \kappa_H^{sy} K_H^x \hat{b}_{K,H} e^{-j(H\beta_0 + \varphi_{K,H}^x)} \right| \\ \varphi_K^x &= Arg\left(\sum_H \kappa_H^{sy} K_H^x \hat{b}_{K,H} e^{-j(H\beta_0 + \varphi_{K,H}^x)} \right) \end{aligned} \tag{11}$$

By load increase one can estimate the fault presence:

- if the harmonic amplitudes measured on both sides of a machine vary in the same direction, then the stator winding does not present an inter-turn short circuit fault,
- if they vary in opposed directions, then this particular failure can be suspected.

Let us point out that the amplitude of the measured harmonics strongly depends on the fault severity and the location of the sensor in relation to the machine. Consequently, taking into account the magnitude of the air-gap flux density and considering the attenuation of these components in the stator core, one will be interested in the components defined by the lowest values of h^s, h^r, k^s, k^r, k'^s, k'^r leading to the smallest as possible value of H [13].

The respect of these constraints leads to consider the spectral line at ω angular frequency $(K=1)$ of magnitude $\hat{b}_{1,1}$. However, this component corresponds to the fundamental of the air-gap flux density which generates the main energetic effects: $\hat{b}_{1,1}$ □ $\hat{b}_{1,H}$ with H different from 1. It results that $\hat{b}_1$ will be not very sensitive to the components defined for $|H|>1$.

The lines are located in a frequency range where they can be easily identified. For induction machine, the analysis is focused on the line at $850\,\text{Hz}$ because it is relative to a flux density component having a low pole pair number as well for the healthy case as for the faulty one.

- for healthy machine: $k^r = 1$, $k^s = -1$, $h^s = 7$ lead to $K = 17, H = -2$ in (4).
- for faulty machine: $k'^r = 1$, $k'^s = -1$, $h^s = 15$ lead to $K_{sc} = 17, H_{sc} = -1$ in (6).

The difference between the both positions is tied to the sign which precedes the component due to the fault. Under healthy conditions the components present the same amplitude, but under faulty conditions, the amplitude of the component in one of the positions increases whereas the other one decreases.

3. FINITE ELEMENT MODEL FOR INDUCTION MOTOR DIAGNOSIS

Finite element model gives much more precise information of the machine than other analytical model under fault conditions [17]. It is based on magnetic field calculation using machine geometry dimensions and materials. In this paper, a time stepping two-dimensional finite element model is performed for modeling analysis of an induction machine with inter-turn fault using FLUX2D software.

3.1. Model of Induction Machine

The FLUX2D circuit, geometry and mesh shown in Figure 4(a)-(c) correspond to the 4 poles squirrel-cage induction motor, 11 kW, 3 x 380 V, f_n = 50 Hz. The 2D computation domain, infinitely extended, contains the stator and the rotor cores - magnetic and nonconductive regions; the 32 rotor bars and 48 stator slots – nonconductive, nonmagnetic and source regions; the air-gap of 0.3 mm thickness and regions of solid conductor type – the rotor slots, the rotor shaft and the motor frame with thickness equal of 8 mm (Figure 4a).

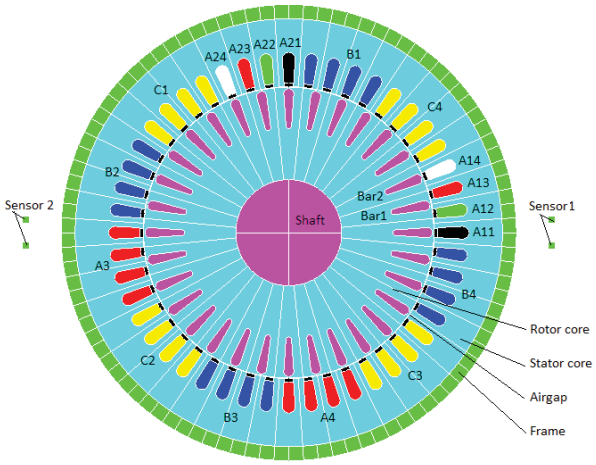

(a)

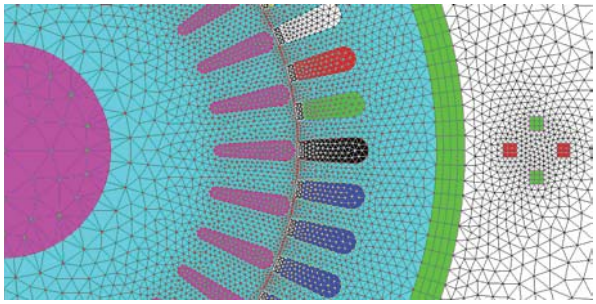

(b)

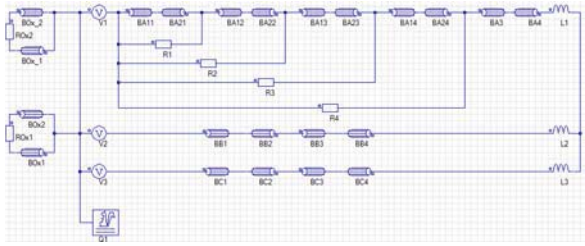

(c)

Figure 4: The finite element model: (a) geometry; (b) mesh zoom; (c) electric circuit.

The state variable of the electromagnetic field - the magnetic vector potential $A(x,y,z,t)$, satisfies the following differential equations[18, 19]:

$$\begin{aligned} &\operatorname{curl}\left[1/\mu \cdot \operatorname{curl} \boldsymbol{A}\right] + \left(\partial \boldsymbol{A}/\partial t\right)/\rho = \boldsymbol{J}_s\left(x,y,z,t\right) \\ &\operatorname{div} \boldsymbol{A} = 0 \end{aligned} \quad (12)$$

where μ is the magnetic permeability, ρ is the resistivity and $\boldsymbol{J}_s$ is the current density in the stator slots. The term $(\partial \boldsymbol{A}/\partial t)/\rho$ is the density of the induced current that is different from zero only in the solid conductor regions of the rotor slots.

The source current density has the structure $\boldsymbol{J}_s[0,0,J_s(x,y,t)]$. As consequence, the vector potential $\boldsymbol{A}_s[0,0,A_s(x,y,t)]$ is oriented along the Oz axis and not depends on the coordinate z and the second equation (12) is implicitly satisfied.

In order to have a good accuracy of the numerical solution the mesh of the computation domain (Figure 4b) is fine enough inside and outside the motor.

Figure 4c gives the electric circuit, attached to the field model which contains the components of stranded coil type, which correspond to the four zones of each of three phases of the stator winding. The phase A is used for study of inter-turn fault, especialy the conductors BA11 and BA21 are schort-circuited by resistance R1 (see Figure 4a). Two coil sensors of 1200 turns are used for study. These sensors correspond to resistances ROx1 and ROx2 (see Figure 4c).

The step-by-step type in time domain analysis of the electromagnetic field considers the time step values 1 ms. The steady state motor operation is reached in

about 0.5 s, but for analysis the time interval (1.8…2) s is considered.
The field-circuit-motion model of the motor takes into account two variants of motor operation: constant rotor speed at no-load operation (1500 rpm), respectively at the load operation (1450 rpm).

3.2. Simulation results

The FFT components at 850 Hz frequency from voltage time variation of E_c measured by the coil sensors (Sensor 1 and 2) in the cases of healthy and faulty machines are presented in Figure 5, respectively in Figure 6. The analysis is focused only on the Ox component.

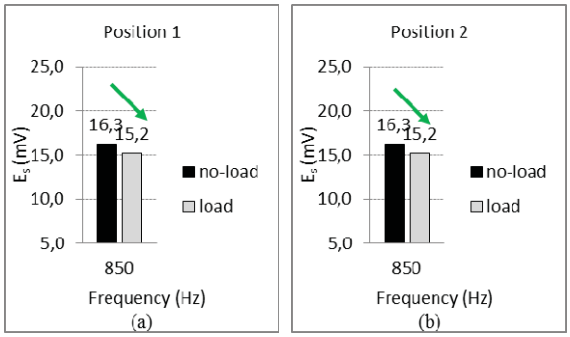

Figure 5: Voltage harmonics at 850 Hz for healthy machine: (a) Position 1; (b) Position 2.

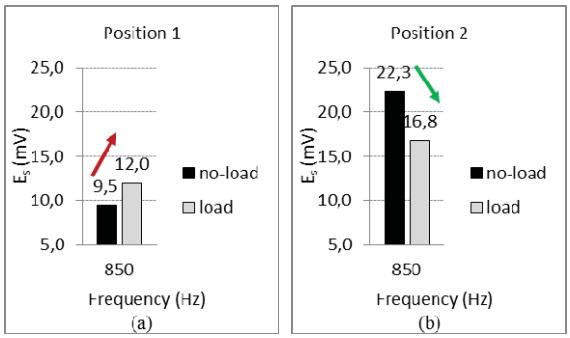

Figure 6: Voltage harmonics at 850 Hz for faulty machine: (a) Position 1; (b) Position 2.

Under healthy conditions (Figure 5) one observe that, the harmonic magnitudes at 850 Hz for two sensors' positions vary in the same way with the load, but under faulty conditions – these magnitudes vary in opposite way with the load (Figure 6).
Also, it can be noticed that the harmonic components at 850 Hz have the same behavior for flux density signals (Figure 7 and 8) measured in the points (X=149 mm; Y=0) and (X=-149 mm; Y=0 mm) situated into sensors' centers.

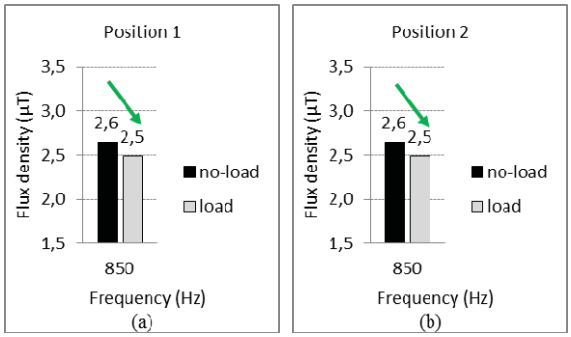

Figure 7: Flux density harmonics at 850 Hz for healthy machine: (a) Position 1; (b) Position 2.

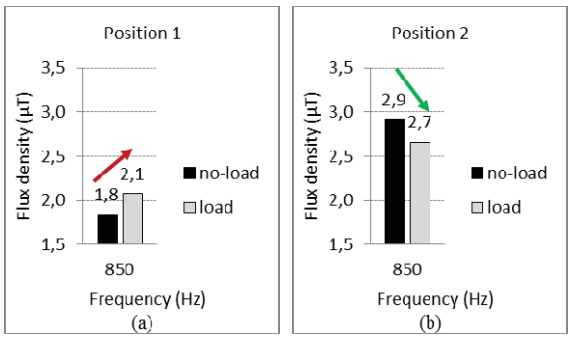

Figure 8: Flux density harmonics at 850 Hz for faulty machine: (a) Position 1; (b) Position 2.

On cane observe that, for the healthy case (Figure 7) at no-load at load conditions the harmonic amplitudes measured on both sides of a machine vary in the same direction. For the faulty machine the harmonic amplitudes vary in opposed directions (Figure 8).
Also, one can remark the same phenomena for EMF and magnetic flux density signals.

4. EXPERIMENTAL RESULTS

In order to validate the results from analytical model, an experimental investigation was realized. The tests was performed on squirrel-cage induction machine characterized by: P = 11 kW; f = 50 Hz; U = 380 V; I_n = 23.2 A; N = 1450 rpm; cosφ = 0.83. This machine has been rewound retaining the original characteristics of the coil so that the terminals of the different stator's elementary sections are extracted from the winding and are brought back to a connector block which is fixed above the machine as indicated in Figure 9. So it is possible to produce short-circuits between elementary coils.

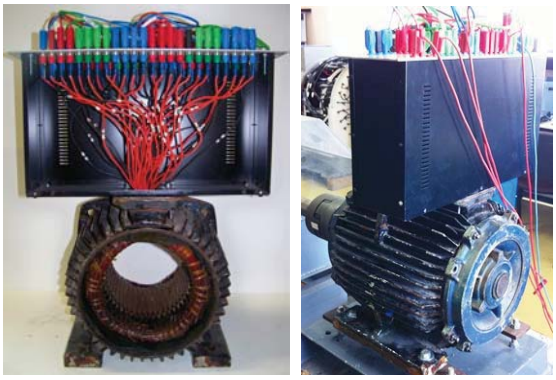

(a) (b)

Figure 9: Modified induction machine

In this case, the stator is star-connected; it has 48 slots and is wound into sections by consequent poles. The inputs and outputs of each elementary coil were deported enough away from the machine frame inside a metal housing to avoid any interference during field measurements near the outer surface of the machine (Figure 9a). Each slot corresponds to a connection terminal which changes color depending on the phase.

Figure 10 shows the winding diagram of the machine with the connections between input and output sections and poles of each phase.

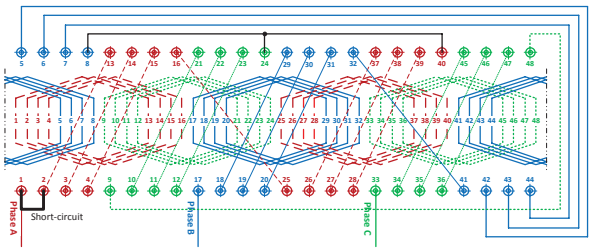

Figure 10: Three phase stator windings of modified induction machine

Consider an elementary section located in the slots numbered k and k'= k+12. The input section is joined to an upper terminal k spotted while its output is connected to a lower terminal denoted by k'. For the elementary section included in the slots k+1 and k'+1, it is used the same method (entry in this section joined to the upper terminal k+1 and output to the lower terminal k'+1). The sections belonging to the same phase are connected in series through these terminals.

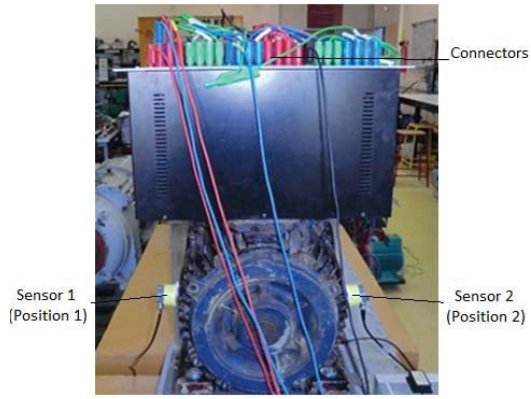

Figure 11: Test-bed used for experimental measurements.

The measurements are made by two simple and non-invasive coil sensors located symmetrically about the machine axis (180° spatially shifted) and placed close to the motor frame between the end bells, roughly in the middle of the machine (Figure 11).

Figure 12 shows the coil sensor with S = 12 cm^2 area, 1200 turns and its frequency response. The EMF signal delivered by this sensor is transmitted to the spectrum analyzer, which performs signal processing and provides its spectrum.

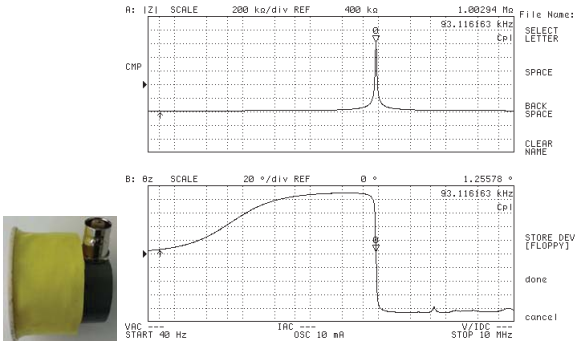

Figure 12: Coil sensor and its frequency response

An elementary coil is short-circuited (terminals 1-2 of a Phase 1 shown in Figure 10). In order to avoid total damage winding, the short-circuit current ($I_{cc} \approx 3I_{Phase1}$) is limited by an external resistance.

One will be interested to the line at $850\,\text{Hz}$ $\left(k^r = \pm 1\right)$.

The results obtained by considering the harmonic of rank $K = K_{sc} = 17$ ($850\,\text{Hz}$ at no-load and load) for two operation forms (motor and generator), are presented in Figure 13 - Figure 16.

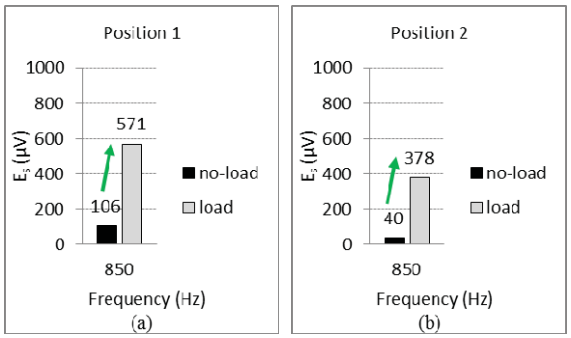

Figure 13: Harmonic components for healthy IM (motor operation) at no-load and load operations for two positions of measurement: (a) Position 1; (b) Position 2.

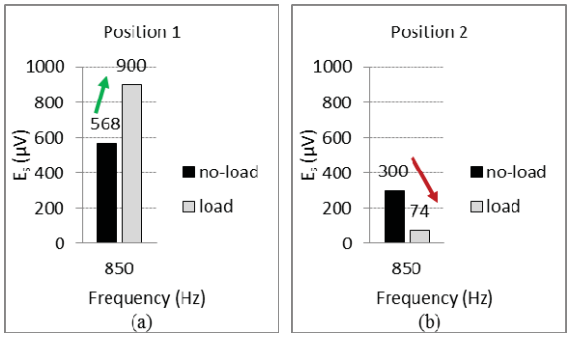

Figure 14: Harmonic components for faulty IM (motor operation) at no-load and load operations for two positions of measurement: (a) Position 1; (b) Position 2.

For motor operation, it can be observe that under healthy case (Figure 13) the harmonic magnitudes at 850 Hz vary in the same ways, but under inter-turn short circuit fault these harmonic magnitudes vary in different ways (Figure 14).

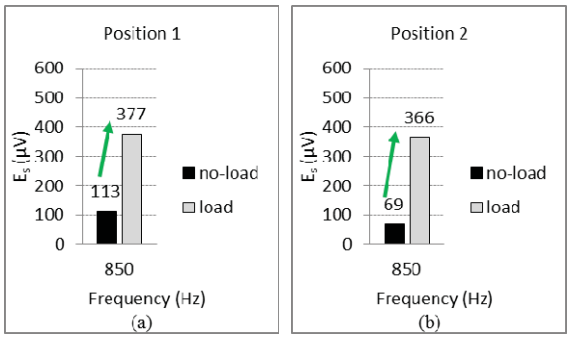

Figure 15: Harmonic components for healthy IM (generator operation) at no-load and load operations for two positions of measurement: (a) Position 1; (b) Position 2.

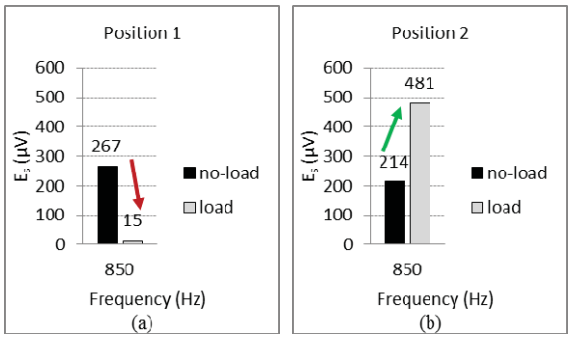

Figure 16: Harmonic components for faulty IM (generator operation) at no-load and load operations for two positions of measurement: (a) Position 1; (b) Position 2.

In the case of generator operation, the same phenomenon can be observed as with motor run:

- under healthy condition – the lines relative to $K = K_{sc} = 17$ (850 Hz) evolve in the same way with the load (Figure 15);
- under faulty condition – these lines evolve in opposite way with the load (Figure 16).

5. CONCLUSIONS

The paper presents an original signature for detection of inter-turn short circuit fault in induction machine using magnetic flux analyses. Under stator winding faults the signature concerns the harmonic at 850 Hz. The method does not require the knowledge of the healthy former state and it is based on comparison between the states at no-load and load operations.
The advantages of proposed non-invasive method compared to other methods are their simplicity to implement, to interpret and a low cost set-up.
The processed EMF signal, delivered by a simple coil sensor, is able to indicate the presence of the fault.
Finally, the experimental tests realized in different operation forms of induction machine (motor and generator) confirm the validation of proposed method. The analytical model is validating by numerical and experimental results.

References

[1] S. Nandi, H. A. Toliyat, and L. Xiaodong, "Condition monitoring and fault diagnosis of electrical motors-a review," *IEEE Transactions on Energy Conversion,* vol. 20, pp. 719-729, December 2005.

[2] W. T. Thomson, "A review of on-line condition monitoring techniques for three-phase squirrelcage induction motors–past, present and future," in *2nd IEEE International Symposium on Diagnostics for Electrical*

Machines, Power Electronics and Drives - SDEMPED '99, Gijon, Spain, 1999, pp. 3-17.

[3] G. B. Kliman, W. J. Premerlani, R. A. Koegl, and D. Hoeweler, "A new approach to on-line turn fault detection in AC motors," in *Industry Applications Conference, 1996. Thirty-First IAS Annual Meeting, IAS '96., Conference Record of the 1996 IEEE*, 1996, pp. 687-693 vol.1.

[4] P. Tavner, L. Ran, J. Penman, and H. Sedding, *Condition Monitoring of Rotating Electrical Machines*, 2 ed. London, United Kingdom: Institution of Engineering and Technology, 2008.

[5] M. E. H. Benbouzid, "Bibliography on induction motors faults detection and diagnosis," *IEEE Transactions on Energy Conversion,* vol. 14, pp. 1065-1074, December 1999.

[6] M. D. Negrea, "Electromagnetic flux monitoring for detecting faults in electrical machines," Doctoral thesis, Electrical and Communications Engineering, Helsinki University of Technology, Helsinki, Finland, 2006.

[7] A. Bellini, F. Filippetti, C. Tassoni, and G. A. Capolino, "Advances in Diagnostic Techniques for Induction Machines," *IEEE Transactions on Industrial Electronics* vol. 55, pp. 4109-4126, December 2008.

[8] F. Filippetti, G. Franceschini, C. Tassoni, and P. Vas, "Recent developments of induction motor drives fault diagnosis using," *IEEE Transactions on Industrial Electronics,* vol. 47, pp. 994-1004, October 2000.

[9] J. Penman and H. Jiang, "The detection of stator and rotor winding short circuits in synchronous generators by analysing excitation current harmonics," in *Opportunities and Advances in International Electric Power Generation, International Conference on (Conf. Publ. No. 419)*, 1996, pp. 137-142.

[10] G. M. Joksimovic and J. Penman, "The detection of inter-turn short circuits in the stator windings of operating motors," *IEEE Transactions on Industrial Electronics,* vol. 47, pp. 1078-1084, October 2000.

[11] A. Stavrou, H. G. Sedding, and J. Penman, "Current monitoring for detecting inter-turn short circuits in induction motors," *IEEE Transactions on Energy Conversion,* vol. 16, pp. 32-37, March 2001.

[12] J. Penman, H. G. Sedding, B. A. Lloyd, and W. T. Fink, "Detection and location of interturn short circuits in the stator windings of operating motors," *IEEE Transactions on Energy Conversion,* vol. 9, pp. 652-658, December 1994.

[13] R. Pusca, R. Romary, A. Ceban, and J.-F. Brudny, "An Online Universal Diagnosis Procedure Using Two External Flux Sensors Applied to the AC Electrical Rotating Machines," *Sensors,* vol. 10, pp. 10448-10466, 2010.

[14] D. Thailly, R. Romary, J.-P. Lecointe, J. F. Brudny, and P. Suau, "Synchronous Machine Diagnosis Using an External Magnetic Flux Sensor," in *XVIIth International Conference on Electrical Machines, ICEM 2006*, Chania, Crete Island, Greece, 2006, pp. 1-6.

[15] R. Romary, R. Corton, D. Thailly, and J. F. Brudny, "Induction machine fault diagnosis using an external radial flux sensor," *The European Physical Journal - Applied Physics,* vol. 32, pp. 125-132, 2005.

[16] R. Romary, D. Roger, and J.-F. Brudny, "Analytical computation of an AC machine external magnetic field," *The European Physical Journal - Applied Physics,* vol. 47, pp. 1-6, 2009.

[17] B. Vaseghi, N. Takorabet, and F. Meibody-Tabar, "Transient finite element analysis of induction machines with stator winding turn fault," *Progress In Electromagnetics Research (PIER) Journals,* vol. 95, pp. 1-18, 2009.

[18] V. Fireţeanu and P. Taraş, "Teaching induction machine through finite element models," in *XVIII International Conference on Electrical Machines - ICEM 2008*, Vilamoura, Portugal, 2008, pp. 1-6.

[19] A. B. J. Reece and T. W. Preston, *Finite Element Methods in Electrical Power Engineering*. Oxford: Oxford University Press, 2000.